Journal Name

ARTICLE TYPE

Cite this: DOI: 00.0000/xxxxxxxxxx

Collective motion of driven semiflexible filaments tuned by soft repulsion and stiffness[†]

Jeffrey M. Moore, a Tyler N. Thompson, a Matthew A. Glaser, and Meredith D. Betterton ab‡

Received Date Accepted Date

DOI: 00.0000/xxxxxxxxxx

In active matter systems, self-propelled particles can self-organize to undergo collective motion, leading to persistent dynamical behavior out of equilibrium. In cells, cytoskeletal filaments and motor proteins self-organize into complex structures important for cell mechanics, motility, and division. Collective dynamics of cytoskeletal systems can be reconstituted using filament gliding experiments, in which cytoskeletal filaments are propelled by surface-bound motor proteins. These experiments have observed diverse dynamical states, including flocks, polar streams, swirling vortices, and single-filament spirals. Recent experiments with microtubules and kinesin motor proteins found that the collective behavior of gliding filaments can be tuned by altering the concentration of the crowding macromolecule methylcellulose in solution. Increasing the methycellulose concentration reduced filament crossing, promoted alignment, and led to a transition from active, isotropically oriented filaments to locally aligned polar streams. This emergence of collective motion is typically explained as an increase in alignment interactions by Vicsek-type models of active polar particles. However, it is not yet understood how steric interactions and bending stiffness modify the collective behavior of active semiflexible filaments. Here we use simulations of driven filaments with tunable soft repulsion and rigidity in order to better understand how the interplay between filament flexibility and steric effects can lead to different active dynamic states. We find that increasing filament stiffness decreases the probability of filament alignment, yet increases collective motion and long-range order, in contrast to the assumptions of a Vicsek-type model. We identify swirling flocks, polar streams, buckling bands, and spirals, and describe the physics that govern transitions between these states. In addition to repulsion and driving, tuning filament stiffness can promote collective behavior, and controls the transition between active isotropic filaments, locally aligned flocks, and polar streams.

1 Introduction

Active particles exhibit complex and dynamical order at length scales much larger than the scale of a single particle. Living systems with collective dynamics include swimming bacteria, schools of fish, flocks of birds, and crowds of people ^{1–6}. The study of active biopolymers is motivated by the activity of cells, because intracellular organization and dynamics are largely governed by the cytoskeleton. Cytoskeletal filaments and motor proteins generate active forces that control the assembly of critical cellular structures and long-range patterns ^{7–9}, or active nematics ^{10,11}. Col-

lective behavior can also occur in filament gliding experiments,

Systems of microtubules propelled by kinesin motors often do not interact and align sufficiently for the emergence of collective motion ^{15,16,18}. Recent work showed that adding methylcellulose as a molecular crowding agent can reduce filament crossing and cause microtubules to locally align ^{18–20}. This has been proposed to occur due to attractive depletion forces that lead filaments to align and form polar bundles ^{10,11,17–23}. Such systems may be well-described by Vicsek-type models of active polar particles, wherein collective motion is governed by local alignment interactions ^{24–28}. However, previous rheological work reported

wherein cytoskeletal filaments are propelled by motor proteins bound to a surface. Previous work on filament gliding has reported several nonequilibrium dynamical states $^{12-17}$. However, our understanding of the physics that controls these phases is incomplete.

^a Department of Physics, University of Colorado, Boulder, CO, 80309, USA.

b Department of Molecular, Cellular, and Developmental Biology, University of Colorado, Boulder, CO 80309, USA. E-mail: mdb@colorado.edu

[†] Electronic Supplementary Information (ESI) available: [details of any supplementary information available should be included here]. See DOI: 00.0000/00000000. ‡ To whom correspondence should be addressed.

that depletion forces alone were insufficient to explain the degree of bundling observed in systems of actin and methylcellulose, and proposed that filaments might be kinetically trapped due to the formation of a methycellulose network²⁹. In addition, microtubule-kinesin gliding experiments observed the alignment of filaments due to local steric interactions in the absence of any depletants, including the formation of self-interacting, singlefilament spirals 15,18,19. Therefore, we seek to understand the phenomenology observed in microtubule-kinesin filament gliding experiments with methylcellulose, in the context of purely repulsive filament interactions that are tunable by the methylcellulose concentration. Most previous theoretical and computational work investigating collective behavior of active filaments with repulsive interactions focused on purely rigid rods ^{30–38} or flexible filaments with hard-core interactions ^{39,40}, but the collective behavior of active semiflexible filaments with tunable steric interactions has not been explored.

In this paper, we study the non-equilibrium phase behavior of active semiflexible polar filaments that interact with a tunable soft repulsive potential. We find that the dynamic state behavior depends on the strength of the repulsive potential, filament rigidity, and activity. Increasing the repulsion leads to a transition between active isotropic filaments and aligned polar streams, matching the alignment behavior observed in experiments with increasing methycellulose concentration ^{18,19}. However, we also find that increasing filament rigidity promotes collective motion while simultaneously decreasing the probability that two intersecting filaments align (Fig. 3, ESI†). This counterintuitive behavior is explained by an increase in directional persistence tuned by increasing filament rigidity. Therefore, our results suggest that while filament alignment by collisions is important, the degree of filament directional persistence is an additional key physical effect contributing to the emergence of collective motion.

2 Model and simulation

Our simulation model expands our previous work on selfpropelled filaments 38,41,42 by adding semiflexibility and tunable repulsion. Our filaments are modeled as inextensible chains of rigid segments, with neighboring segments subject to bending forces to enforce the filament persistence length L_p (Fig. 1A). The filament equations of motion are implemented using the constrained Brownian dynamics algorithm of Montesi, Morse, and Pasquali 43 for a semiflexible chain with anisotropic friction. Each segment of the filament experiences random forces so that its dynamics obey the fluctuation-dissipation theorem for slender filaments at thermal equilibrium 44. Our choice of filament model has the advantage of being inherently inextensible, and lacks a dependence on large harmonic forces that are typically required to model stiff filaments (see ESI†). This allows us to model microtubules, which are inextensible and have high persistence lengths $L_p/L \approx 100-1000^{45}$, but nevertheless often appear bent in both in vivo and in vitro, indicating the importance of their flexibilitv^{46–48}.

The activity of motor proteins is modeled by a polar driving force per unit length $f_{\rm dr}$ tangent to each filament segment. This choice reflects experimental observations that filament velocity is

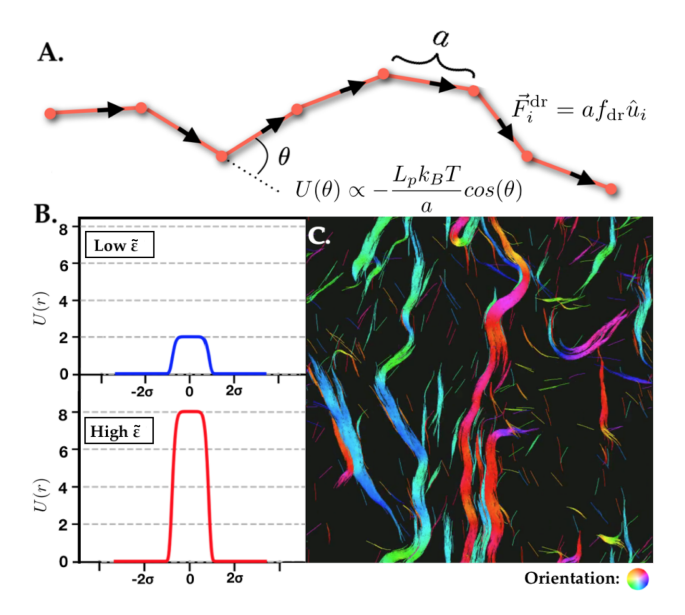


Fig. 1 Model schematic and simulation snapshot. A) Schematic of self-propelled, semiflexible inextensible, filaments, which contain rigid segments of length a with a bending potential between adjacent segments $U(\theta)$. The segment length used in our simulations is chosen to be as small as possible while maintaining numerical stability of the simulations, and is typically in the range of 1–4 σ depending on the persistence length (see ESI†). Each segment experiences a parallel driving force $F_{\rm dr}$. B) Plot of the repulsive potential U(r) centered on a filament of diameter σ . C) Snapshot of a simulation with packing fraction $\phi=0.2$, filament rigidity $\tilde{\kappa}=100$, and repulsion $\tilde{\epsilon}=6$.

constant and independent of methycellulose concentration, even during filament crossing events ^{15,20}, suggesting that stochastic effects due to the motors (e.g., binding and unbinding, variation in motor stepping) occur at short enough time scales so as to not significantly alter large-scale behavior.

Interactions between filaments are repulsive but soft, defined by the generalized exponential potential (GEM-8), $U(r)=\varepsilon e^{-(r/\sigma)^8}$, with cutoff $U(r>\sqrt{2}\sigma)=0$. Here r is the minimum distance between neighboring segments and σ the diameter of a filament (Fig. 1B). The maximum potential value ε represents the energy required for two segments to overlap. This potential is steep near the edge of a filament. Interactions occur between each filament segment, except for nearest-neighbor segments of the same filament. While filaments experience local drag, we neglect long-range hydrodynamic interactions because previous experiments found these forces to be negligible 19 .

Filaments are inserted at a packing fraction $\phi = A_{\rm fil}/A_{\rm sys}$, where $A_{\rm sys}$ is the area of the simulation box and $A_{\rm fil} = N(L\sigma + \pi\sigma^2)$ is the total area occupied by N spherocylindrical filaments of length L and diameter σ . The characteristic timescale is the time for a filament to move the distance of its contour length, $\tau_A = L/v$, with the velocity depending on the total driving force and the coefficient of friction acting parallel to the filament, $v = \xi_{\parallel}^{-1} F_{\rm dr}$. The filament driving force per unit length is set by the Péclet number, which is the ratio of active and diffusive transport time scales, $P = \tau_D/\tau_A = f_{\rm dr} L^2/k_B T$. We explore the range $P = 10^4 - 10^5$, based on calculations of active forces in experiments 15 (see ESI†). Simulations were run for $10^3 - 10^4 \tau_A$.

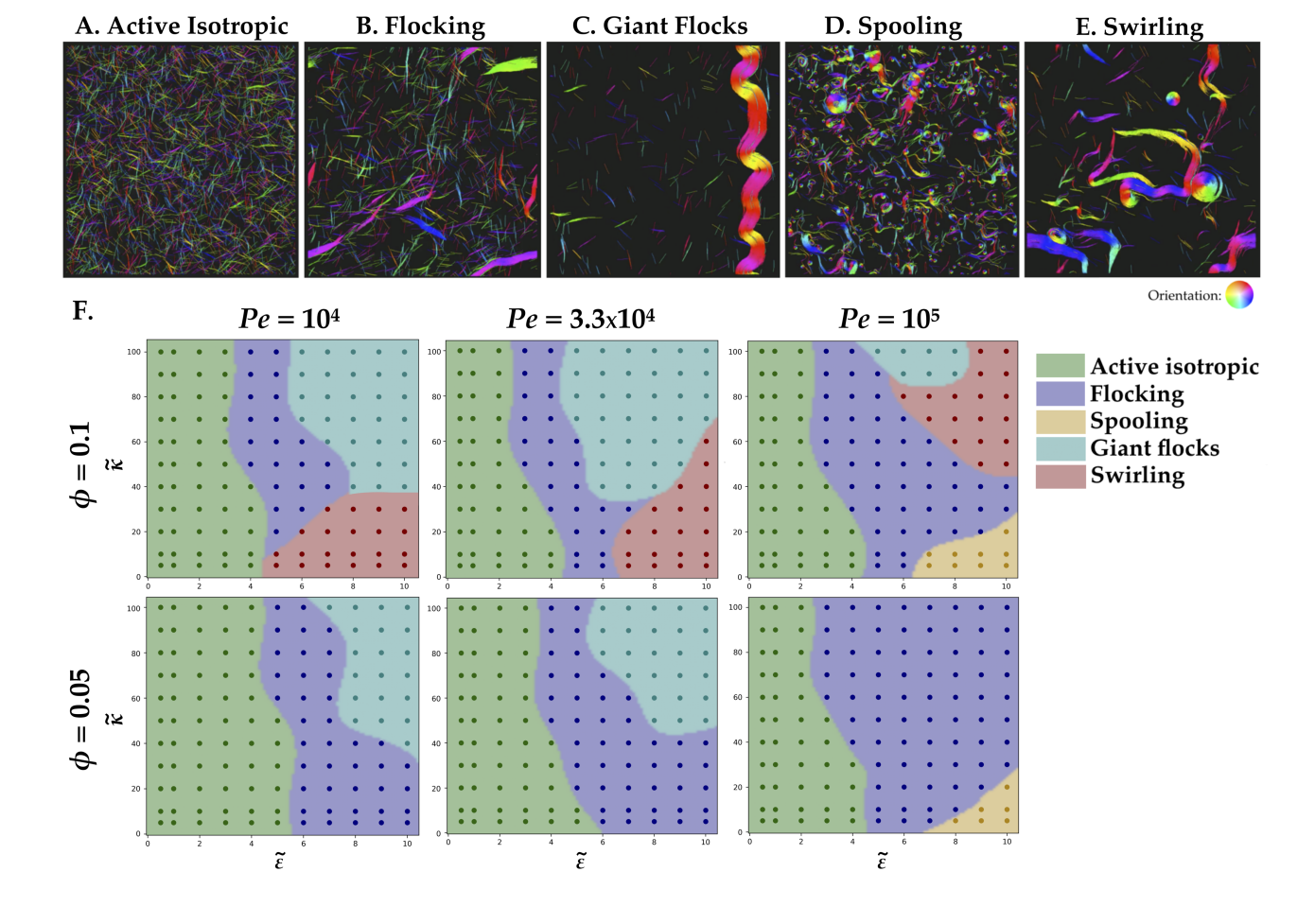


Fig. 2 Simulation snapshots and phase diagram. A) Active isotropic ($\phi=0.2$, $\tilde{\epsilon}=1.5$, $\tilde{\kappa}=50$). B) Flocking ($\phi=0.2$, $\tilde{\epsilon}=2$, $\tilde{\kappa}=100$). C) Polar band ($\phi=0.2$, $\tilde{\epsilon}=5$, $\tilde{\kappa}=100$). D) Spooling ($\phi=0.2$, $\tilde{\epsilon}=10$, $\tilde{\kappa}=20$). E) Swirling ($\phi=0.2$, $\tilde{\epsilon}=10$, $\tilde{\kappa}=100$). F) Phase diagram of self-propelled semiflexible filaments with varying rigidity $\tilde{\kappa}$ and repulsion $\tilde{\epsilon}$ for Péclet number Pe = 10^4-10^5 , and packing fraction $\phi=0.05-0.1$. Points represent simulations; background colors are for visualization of clusters. Separation of phases was achieved through high-dimensional clustering of the simulation order parameters (see ESI†).

Our results depend on six dimensionless parameters: rigidity $\tilde{\kappa} = L_p/L$, interaction energy $\tilde{\varepsilon} = \varepsilon/\varepsilon_{\rm dr}$, packing fraction $\phi =$ $A_{\rm fil}/A_{\rm sys}$, aspect ratio $l=L/\sigma=60$, system size $l_{\rm sys}=L_{\rm sys}/L=20$, and Péclet number Pe. The interaction energy has been rescaled by ε_{dr} , which is the energy required for the potential to exert a maximum force equal to the driving force of a particle with length σ . Our simulation varies $\tilde{\kappa}$ from 5–1000; previous computational work on active semiflexible filaments examined the range $\tilde{\kappa} < 20^{39,40}$, however this is not well-suited for the study of microtubules, which can have $\tilde{\kappa} \approx 100\text{--}1000$. We varied $\tilde{\epsilon}$ from 1-20, corresponding to filament pair-alignment behavior estimated from previous gliding assay experiments ^{18–20} (Fig. 3). The work here focuses on the low-density regime of $\phi = 0.05$, 0.1, but we also explored higher filament densities ($\phi = 0.2, 0.4, \text{ and } 0.8$) at $Pe = 10^5$ (see ESI†). Although the filament aspect ratio is fixed, varying the filament rigidity is analogous to varying the length of a filament with a fixed persistence length.

3 Results

Our simulations generated five primary phases: active isotropic, flocking, giant flocking, swirling, and spooling (Fig. 2). To quantify the dynamical phases, we used six global order parameters: the polar order P, nematic order Q, average contact number c, average local polar order p, average spiral number s, and number fluctuations ΔN (see ESI†). We also quantified the collective dynamics of the system by characterizing the flocking behavior in terms of the number of flocking filaments N_F/N , and frequencies that filaments joined or left a flocking state, respectively f_{NF-F} and f_{F-NF} . Using a high-dimensional clustering algorithm, we identified 5 clusters in this nine-dimensional order parameter space corresponding to the different phases observed for our range of parameters (see ESI†).

In the active isotropic phase, filaments cross each other in all directions, resembling filament gliding experiments that do not exhibit collective motion (Fig. 2A). The flocking phase is characterized by the coexistence of multiple polar domains of aligned filaments (Fig. 2B). Flocks are dynamic, with filaments continu-

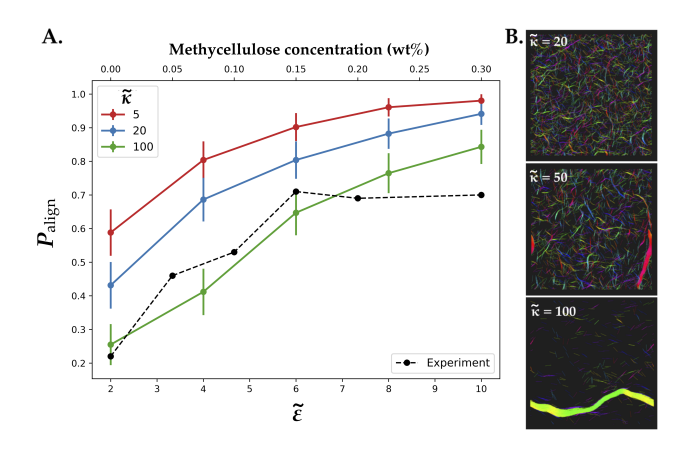


Fig. 3 A) Plot of the probability for two filaments to align upon collision for Pe = 10^5 . Increasing repulsion $\tilde{\epsilon}$ increases P_{align} while increasing rigidity $\tilde{\kappa}$ decreases it. Experimental values taken from Saito et. al 19 with corresponding methylcellulose concentration as the top x-axis. B) Simulation snapshots illustrating how increasing filament rigidity increases collective motion. All images show simulations with $\tilde{\epsilon}=5$, $\phi=0.1$, Pe = 10^5 .

ously joining and leaving the flocking state. The giant flocking phase occurs when all flocks in the system coalesce into a single dominating flock, and exhibits long-range order. At higher densities, giant flocks can span the system length (Fig. 2C), and can be either one band ($\phi=0.1$ –0.2) or many counter-propagating bands ($\phi=0.4$ –0.8). In the spooling phase, filaments are flexible enough to self-interact, and many filaments form spirals (Fig. 2D). The swirling phase contains large, swarming flocks that collide, self-interact, and form transient vortices (Fig. 2E).

Collective motion emerges with increasing repulsion or rigidity. When both filament repulsion and rigidity are small, we find the active isotropic phase at all densities and Péclet numbers (Fig. 2F). Self-organization and collective motion can occur by increasing either repulsion or stiffness; increasing $\tilde{\epsilon}$ tends to increase collective behavior, while increasing $\tilde{\kappa}$ or ϕ tends to increase long-range order. Previous experimental work has found that the transition from an active isotropic phase to polar streams was driven by an increase in alignment events between pairs of colliding filaments 16,18-20. Accordingly, we measured the correlation between the emergence of collective behavior and the probability of filament alignment, P_{align} (see ESI†). We find that P_{align} increases monotonically with increasing repulsion, in agreement with trends in experiments for increasing methylcellulose concentrations $^{18-20}$ (Fig. 3). In contrast, P_{align} decreases monotonically with increasing stiffness (see ESI†). Remarkably, we found regions of phase space where increasing stiffness drives the emergence of collective motion, and regions where increasing repulsion inhibits long-range organization and collective behavior.

The negative correlation between $P_{\rm align}$ and filament rigidity can be understood by considering the additional energy required to apply a torque on a stiff filament. Flexible filaments need only bend very marginally at the leading end to align during a collision. Stiff filaments cannot bend as easily and thus require additional torque to align. Higher torques between colliding filaments would increase overall alignment in the case of hard-core repulsive interactions 32 . However, with a finite repulsivity, the higher

energy cost leads to a reduction in the probability of alignment.

The counterintuitive result that increasing stiffness lowers collisional alignment but increases collective motion reflects a tradeoff between filament alignment and the directional persistence of filament trajectories. The directional persistence of filaments is quantified by measuring the autocorrelation of filament orientation u, $C(t) = \langle u(0) \cdot u(t) \rangle$. The result can be fitted to a decaying exponential with characteristic timescale τ , with a high τ corresponding to a high degree of directional persistence. The directional persistence was measured for filaments at different rigidities and Péclet numbers in the absence of interactions (see ESI†). Since driven filaments are readily deflected from their trajectories by small deviations of the leading filament tip, rigid filaments that resist deflection exhibit longer orientation correlation times, and thus have a greater directional persistence than flexible filaments. Flocking filaments that move ballistically have longer-lived alignment and thus a higher flocking lifetime, permitting other filaments to join. Although the frequency of alignment may be lower for stiff filaments, the longer duration of alignment compensates for the low alignment probability. In contrast, flexible filaments have a higher rate of alignment, leading to the rapid creation of polar clusters (Fig. 4), but they are easily deflected away, resulting in short-lived flocks. Thus, flexible filaments require a larger $\tilde{\epsilon}$ to cross the active isotropic-flocking boundary. Our results suggest that filament alignment and directional persistence are both important for the emergence of collective motion and stable flocks.

The flocking phase consists of multiple polar domains of aligned filaments, with individual flocks characterized by high local filament density and local polar order p. Individual flocking filaments are identified by the criterion $p_i>0.5$, with filaments that are located in the flock interior exhibiting high contact number c_i as well. The number of flocking filaments increases with filament stiffness and repulsivity. Filaments with lower $\tilde{\kappa}$ have faster switching between flocking and non-flocking states compared to stiff filaments, yet the saturation of the number of flocking filaments occurs at high $\tilde{\kappa}$ and slow switching frequencies (Fig. 4).

With increasing stiffness, flocks that form in a transient flocking phase can coalesce into a single dominating flock, characteristic of the giant flock phase. In the giant flock phase, the number of flocking filaments saturates, depriving the remaining system of the necessary filament density to form additional stable flocks. Giant flocks in this phase are characteristically long and narrow, allowing them to efficiently intersect with and capture non-flocking filaments. The rate of switching between flocking and non-flocking states becomes low in the giant flock phase, due to the large number of filaments that are kinetically trapped in the flock interior (see ESI†). Giant flocks are more stable at lower driving, consistent with previous reports that high activity can inhibit collective behavior of filaments with flexibility³⁹. Due to finite-size effects of the simulation, the continued growth of the giant flock at higher densities ($\phi \ge 0.1$) will often lead it to span the length of the system, $L_{\rm flock} > 20L$, ending with the formation of a persistent polar band. At very high densities ($\phi \ge 0.4$), multiple independent bands can form simultaneously, resulting

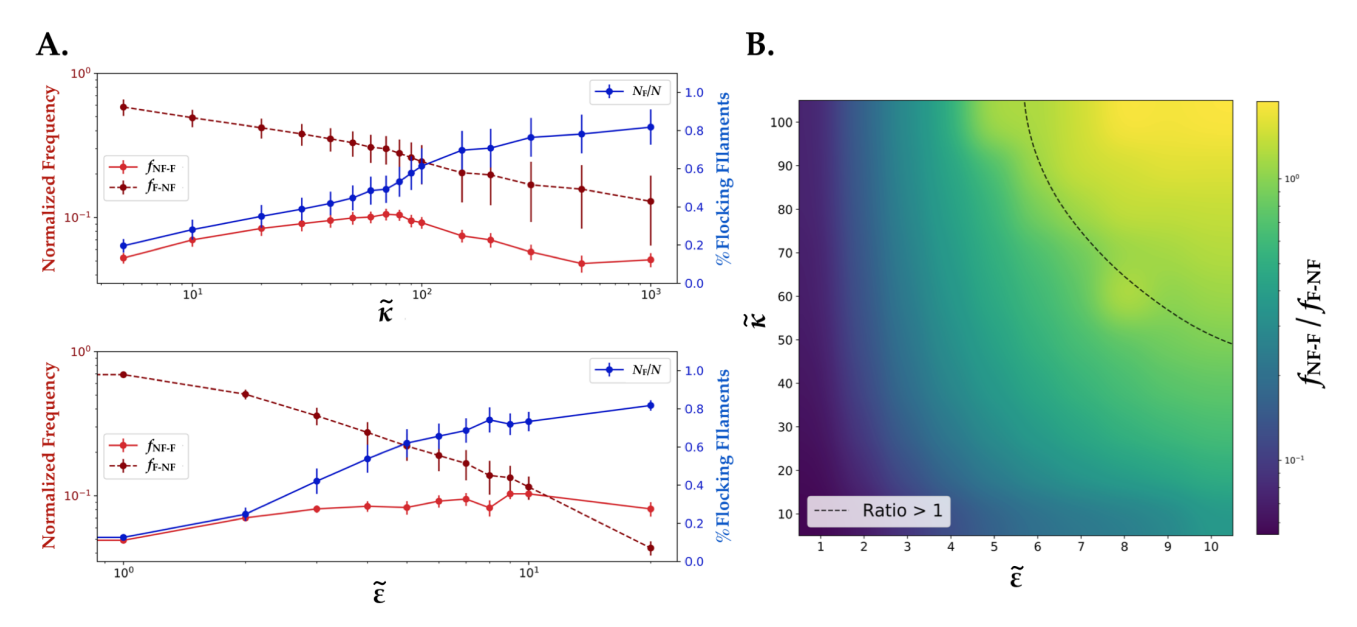


Fig. 4 A) Switching frequency between the flocking (F) and not-flocking (NF) states plotted as a function of filament rigidity (top) and soft repulsion strength (bottom) averaged over all simulations with $\phi=0.1$, Pe = 10^5 , and time-averaged for the final 10% of the simulation. The frequency is normalized by the population of filaments available in the initial state, and plotted alongside the percentage of filaments that are flocking in the system. The frequencies have units τ_A^{-1} (see ESI†). B) Plot of the ratio of the flocking state switching frequency ratio $f_{\rm NF-F}/f_{\rm F-NF}$ with respect to $\tilde{\kappa}$ and $\tilde{\epsilon}$ for $\phi=0.1$, Pe = 10^5 . The region where the frequency for joining a flock is greater than the departure frequency is indicated by the dashed line.

in coexisting nematic bands. We note that high filament density paired with high $\tilde{\kappa}$ results in a stable giant flock phase even at low $\tilde{\epsilon}$. The high local filament densities serve to restrict the rotational degrees of freedom of gliding filaments, further increasing directional persistence and the stability of polar bands.

Our phase diagram shows a limited region of stability for long-range collective motion in the giant flocking phase. This occurs because although increasing $\tilde{\kappa}$ promotes long-range order, increasing $\tilde{\epsilon}$ too high can break it. At high $\tilde{\kappa}$ and high $\tilde{\epsilon}$, collisions cause large deformations of flocking and banding filaments, leading to buckling. In the simulation shown in Fig. 2C, the filaments repeatedly form a polar band, which buckles, shears, falls apart, and eventually reforms. Similar dynamic phases have been observed in systems of self-propelled rods 33 and semiflexible filaments driven by motors 40 . Therefore, only intermediate values of $\tilde{\epsilon}$ facilitate persistent long-range order as giant flocks.

While increasing $\tilde{\epsilon}$ typically increases alignment events, promoting collective motion, for flexible filaments (low $\tilde{\kappa}$), filaments can bend and self-interact via collisions to form spirals (Fig. 5C). Spirals are seen at all Péclet numbers, but are increasingly stable with higher driving. Stable single-filament spirals can persist until a collision with another filament or flock deforms the filament enough to release it. At high driving, the system can enter the spooling phase, wherein a majority of filaments become kinetically trapped as spirals. The spooling phase resembles the frozen, active steady states found in previous experimental work ¹⁴. The principle mechanism of spool formation has been of significant interest ^{15,39,49–53}, with suggestions ranging from defects in the motor lattice to thermal activation. Previous experiments with microtubules and dynein have observed stable filament vortices attributed to filament curvature induced by motors ¹⁶, which are

absent in our simulations. The spooling phase demonstrated here is governed by steric self-interactions and collisions, as found in previous modeling work ^{39,51}. Their overwhelming appearance at high driving may be due to a rescaling of the effective filament rigidity at high activity, which has been reported in other recent work ^{51,54–56}, leading to an apparent softening of the filament that may contribute to a buckling instability ⁵⁷ (see ESI†). Therefore, while spool formation in experiments may have contributions from defects in the protein lattice, pinning of filaments by dead motors, or intrinsic curvature, our results indicate that these mechanisms are not necessary for spool formation.

When repulsion and stiffness are both high, even transient polar bands can no longer form, and the system enters the swirling phase. High-energy collisions due to large bending and repulsive forces cause large deformation of flocks, leading to shorter end-to-end flock length and inhibiting the long-range order that is present at lower interaction energy. Flocks in the swirling phase can have much shorter aspect ratios compared to giant flocks. The sharp bending of flocks can result in flock self-interaction, which may form a large, transient vortex of filaments (Fig. 5D).

Our simulations do not display symmetry breaking of the system chirality as observed in some previous work 14,16,20 , due to zero preferred filament curvature in our model. When an intrinsic curvature is added with simulation parameters that otherwise form stable polar bands, we observe a rotation in the polar order vector (see ESI †), similar to previous simulations of gliding filaments with intrinsic curvature 20 .

4 Conclusions

We have examined of the role of flexibility and repulsivity in the collective behavior of active polar filaments. The phase diagram

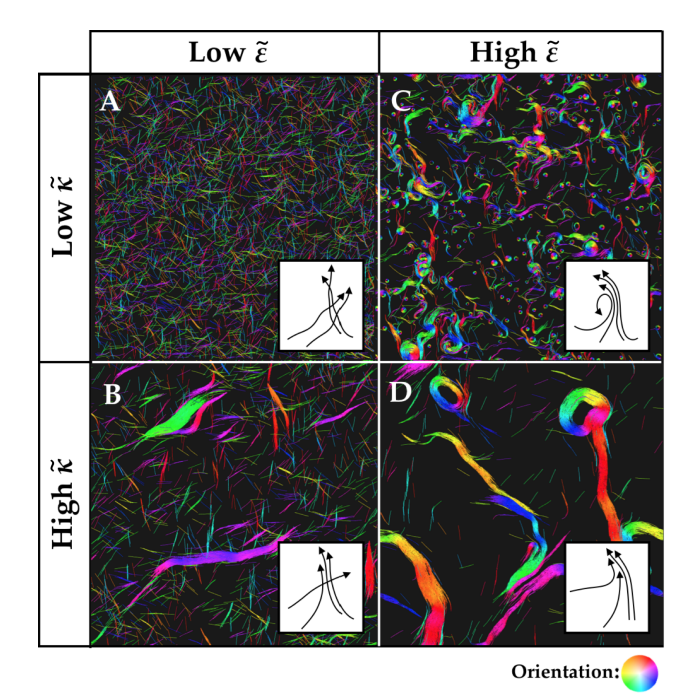


Fig. 5 Diagram depicting the phase behavior of active filaments with varying rigidity $\tilde{\kappa} = 20,100$ and repulsion $\tilde{\epsilon} = 2,10$ at $\phi = 0.2$ and Pe = 10⁵. Increasing repulsion decreases the probability of filament crossing. Increasing filament rigidity increases polar order of flocks and increases resistance to filament bending in collisions.

presented here makes predictions that could guide future experiments seeking to observe collective behavior in systems of active semiflexible polymers. These systems can exhibit a wide variety of active, dynamic states, with transitions that are controllable by tuning repulsive interactions and filament rigidity. The ability to control the transition between these states may have applications for drugs targeting cortical cytoskeletal filaments or nanodevices that use cytoskeletal filaments as molecular shuttles ^{58,59}.

Conflicts of interest

There are no conflicts to declare.

Acknowledgements

We would like to thank Michael Stefferson for helpful discussions. This work was funded by the Soft Materials Research Center under NSF MRSEC Grant No. DMR-1420736, and the National Science Foundation under NSF GRFP Award No. DGE-1144083 and NSF Grant No. DMR-1725065. This work utilized the RMACC Summit supercomputer, which is supported by the National Science Foundation (awards ACI-1532235 and ACI-1532236), the University of Colorado Boulder, and Colorado State University. The Summit supercomputer is a joint effort of the University of Colorado Boulder and Colorado State University.

Notes and references

- 1 T. Vicsek and A. Zafeiris, *Physics Reports*, 2012, **517**, 71–140.
- 2 A. Czirók, E. Ben-Jacob, I. Cohen and T. Vicsek, Physical Review E, 1996, 54, 1791-1801.
- 3 C. Dombrowski, L. Cisneros, S. Chatkaew, R. E. Goldstein and J. O. Kessler, Physical Review Letters, 2004, 93, 098103.

- 4 J. K. Parrish, S. V. Viscido and D. Grünbaum, The Biological Bulletin, 2002, 202, 296-305.
- 5 I. L. Bajec and F. H. Heppner, Animal Behaviour, 2009, 78, 777-789.
- 6 J. L. Silverberg, M. Bierbaum, J. P. Sethna and I. Cohen, *Phys*ical Review Letters, 2013, 110, 228701.
- 7 A. A. Hyman and E. Karsenti, Cell, 1996, 84, 401–410.
- 8 F. J. Nedelec, T. Surrey, A. C. Maggs and S. Leibler, Nature, 1997, 389, 305-308.
- 9 T. Surrey, F. Nédélec, S. Leibler and E. Karsenti, Science, 2001, **292**, 1167–1171.
- 10 T. Sanchez, D. T. N. Chen, S. J. DeCamp, M. Heymann and Z. Dogic, Nature, 2012, 491, 431-434.
- 11 L. M. Lemma, S. J. DeCamp, Z. You, L. Giomi and Z. Dogic, Soft Matter, 2019, 15, 3264-3272.
- 12 T. Butt, T. Mufti, A. Humayun, P. B. Rosenthal, S. Khan, S. Khan and J. E. Molloy, Journal of Biological Chemistry, 2010, **285**, 4964–4974.
- 13 V. Schaller, C. Weber, C. Semmrich, E. Frey and A. R. Bausch, Nature, 2010, 467, 73-77.
- 14 V. Schaller, C. A. Weber, B. Hammerich, E. Frey and A. R. Bausch, Proceedings of the National Academy of Sciences, 2011, 108, 19183-19188.
- 15 L. Liu, E. Tüzel and J. L. Ross, Journal of Physics: Condensed Matter, 2011, 23, 374104.
- 16 Y. Sumino, K. H. Nagai, Y. Shitaka, D. Tanaka, K. Yoshikawa, H. Chaté and K. Oiwa, Nature, 2012, 483, 448-452.
- 17 L. Huber, R. Suzuki, T. Krüger, E. Frey and A. R. Bausch, Science, 2018, 361, 255-258.
- 18 D. Inoue, B. Mahmot, A. M. Rashedul Kabir, T. Ishrat Farhana, K. Tokuraku, K. Sada, A. Konagaya and A. Kakugo, Nanoscale, 2015, 7, 18054-18061.
- 19 A. Saito, T. Ishrat Farhana, A. M. Rashedul Kabir, D. Inoue, A. Konagaya, K. Sada and A. Kakugo, RSC Advances, 2017, 7, 13191-13197.
- 20 K. Kim, N. Yoshinaga, S. Bhattacharyya, H. Nakazawa, M. Umetsu and W. Teizer, Soft Matter, 2018, 14, 3221-3231.
- 21 S. Asakura and F. Oosawa, Journal of Polymer Science, 1958, **33**, 183–192.
- 22 D. Marenduzzo, K. Finan and P. R. Cook, The Journal of Cell Biology, 2006, 175, 681âĂŞ686.
- 23 A. W. C. Lau, A. Prasad and Z. Dogic, EPL (Europhysics Letters), 2009, 87, 48006.
- 24 T. Vicsek, A. Czirók, E. Ben-Jacob, I. Cohen and O. Shochet, Physical Review Letters, 1995, 75, 1226-1229.
- 25 H. Levine, W.-J. Rappel and I. Cohen, *Physical Review E*, 2000, **63**, 017101.
- 26 G. Grégoire and H. Chaté, Physical Review Letters, 2004, 92,
- 27 M. Aldana, V. Dossetti, C. Huepe, V. M. Kenkre and H. Larralde, Physical Review Letters, 2007, 98, 095702.
- 28 H. Chaté, F. Ginelli, G. Grégoire and F. Raynaud, Physical Review E, 2008, 77, 046113.

- 29 S. KÃűhler, O. Lieleg and A. R. Bausch, *PLoS ONE*, 2008, **3**, year.
- 30 P. Kraikivski, R. Lipowsky and J. Kierfeld, *Physical Review Letters*, 2006, **96**, 258103.
- 31 F. Peruani, A. Deutsch and M. BÃd'r, *Physical Review E*, 2006, **74**, 030904.
- 32 A. Baskaran and M. C. Marchetti, *Physical Review Letters*, 2008, **101**, 268101.
- 33 F. Ginelli, F. Peruani, M. Bär and H. Chaté, *Physical Review Letters*, 2010, **104**, 184502.
- 34 Y. Yang, V. Marceau and G. Gompper, *Physical Review E*, 2010, **82**, 031904.
- 35 F. Peruani, T. Klauss, A. Deutsch and A. Voss-Boehme, *Physical Review Letters*, 2011, **106**, 128101.
- 36 F. Peruani, J. Starruß, V. Jakovljevic, L. Søgaard-Andersen, A. Deutsch and M. Bär, *Physical Review Letters*, 2012, 108, 098102.
- 37 M. Abkenar, K. Marx, T. Auth and G. Gompper, *Physical Review E*, 2013, **88**, 062314.
- 38 H.-S. Kuan, R. Blackwell, L. E. Hough, M. A. Glaser and M. D. Betterton, *Physical Review E*, 2015, **92**, year.
- 39 Ö. Duman, R. E. Isele-Holder, J. Elgeti and G. Gompper, *Soft Matter*, 2018, **14**, 4483–4494.
- 40 G. Vliegenthart, A. Ravichandran, M. Ripoll, T. Auth and G. Gompper, *arXiv:1902.07904* [cond-mat], 2019.
- 41 T. Gao, R. Blackwell, M. A. Glaser, M. D. Betterton and M. J. Shelley, *Physical Review Letters*, 2015, **114**, 048101.
- 42 J. M. Moore, *C-GLASS: A Coarse-Grained Living Active Systems Simulator*, 2020, https://zenodo.org/record/3841613#.Xsm7mcZMEcg, 10.5281/zenodo.3841613.
- 43 A. Montesi, D. C. Morse and M. Pasquali, *The Journal of Chemical Physics*, 2005, **122**, 084903.
- 44 M. Doi and S. F. Edwards, The Theory of Polymer Dynamics,

- Clarendon Press, 1988.
- 45 F. Gittes, B. Mickey, J. Nettleton and J. Howard, *Journal of Cell Biology*, 1993, **120**, 923âĂŞ934.
- 46 D. J. Odde, L. Ma, A. H. Briggs, A. DeMarco and M. W. Kirschner, *Journal of Cell Science*, 1999, **112**, 3283åÄŞ3288.
- 47 C. P. Brangwynne, F. C. MacKintosh, S. Kumar, N. A. Geisse, J. Talbot, L. Mahadevan, K. K. Parker, D. E. Ingber and D. A. Weitz, *Journal of Cell Biology*, 2006, **173**, 733âĂŞ741.
- 48 J. L. McGrath, Current Biology, 2006, 16, R800âĂŞR802.
- 49 I. Luria, J. Crenshaw, M. Downs, A. Agarwal, S. Banavara Seshadri, J. Gonzales, O. Idan, J. Kamcev, P. Katira, S. Pandey, T. Nitta, S. R. Phillpot and H. Hess, *Soft Matter*, 2011, 7, 3108–3115.
- 50 A. T. Lam, C. Curschellas, D. Krovvidi and H. Hess, *Soft Matter*, 2014, **10**, 8731–8736.
- 51 R. E. Isele-Holder, J. Elgeti and G. Gompper, *Soft Matter*, 2015, **11**, 7181–7190.
- 52 V. VanDelinder, S. Brener and G. D. Bachand, *Biomacromolecules*, 2016, **17**, 1048–1056.
- 53 Z. Mokhtari and A. Zippelius, *Physical Review Letters*, 2019, **123**, 028001.
- 54 S. K. Anand and S. P. Singh, *Physical Review E*, 2018, **98**, 042501.
- 55 N. Gupta, A. Chaudhuri and D. Chaudhuri, *Physical Review E*, 2019, **99**, 042405.
- 56 M. S. E. Peterson, M. F. Hagan and A. Baskaran, Journal of Statistical Mechanics: Theory and Experiment, 2020, 2020, 013216.
- 57 R. E. Isele-Holder, J. JÃďger, G. Saggiorato, J. Elgeti and G. Gompper, *Soft Matter*, 2016, **12**, 8495âĂŞ8505.
- 58 T. Nitta, A. Tanahashi, M. Hirano and H. Hess, *Lab on a Chip*, 2006, **6**, 881–885.
- 59 H. Hess, Annual Review of Biomedical Engineering, 2011, 13, 429–450.